Journal of Asian Earth Sciences 107 (2015) 232–243

Contents lists available at ScienceDirect

Journal of Asian Earth Sciences

journal homepage: www.elsevier.com/locate/jseaes

Earthquake potential of the Sichuan-Yunnan region, western China

Fan Wang [a,b], Min Wang [a], Yanzhao Wang [a], Zheng-Kang Shen [c,d,*]

[a] State Key Laboratory of Earthquake Dynamics, Institute of Geology, China Earthquake Administration, Beijing 100029, China
[b] National Geomatics Center of China, Beijing 100830, China
[c] Department of Earth, Planetary, and Space Sciences, University of California, Los Angeles, CA 90095-1567, USA
[d] Department of Geophysics, Peking University, Beijing 100871, China

ARTICLE INFO

Article history:
Received 16 October 2014
Received in revised form 10 April 2015
Accepted 21 April 2015
Available online 9 May 2015

Keywords:
Seismic hazard
Sichuan-Yunnan region
Seismic moment accumulation
Strain rate
Earthquake catalog

ABSTRACT

We estimate the seismic hazard potential in the Sichuan-Yunnan region, western China using three different approaches. Our first approach, based on the assumption that the earthquake probability is proportional to the past seismicity rate, uses a regional earthquake catalog to constrain the probability model. A retrospective test shows that the 'forecasts' have some predictive power for strong events occurred on fault segments with shorter earthquake recurrence time, but not for that with longer recurrence time such as the Longmenshan fault. Our second approach, based on the assumption that the earthquake probability is proportional to crustal strain rate, uses secular geodetic strain rate deduced from GPS velocity data to constrain the probability model. A retrospective test of the model with earthquake occurrence of the past 30 years shows that the model 'forecasted' poorly. However, the model seems to 'forecast' spatial intensity of earthquakes for the past 500 years reasonably well, suggesting that the geodetic strain rate obtained at the decadal scale may still be a good indicator of long term earthquake activity in the region, but only at a time scale of hundreds of years. Our third approach uses GPS velocity data to determine the seismic moment accumulation rates on major faults, and a historical earthquake catalog to estimate seismic moments released in the past. Comparison of the two yields estimates of present day seismic moments cumulated on major faults, and a retrospective test shows some predictive power of the method. Our result suggests that numerous faults in the Sichuan-Yunnan region have cumulated seismic moments capable of producing $M > 7.5$ earthquakes, including the Xiaojiang, Jiali, Northern Nujiang, Nandinghe, and Red River–Puer faults, and the junction fault between the Xianshuihe and Ganzi-Yushu faults.

1. Introduction

The Sichuan-Yunnan region (97–108°E, 21–33°N) is located at the southeast margin of the Tibetan plateau (Fig. 1). Being manifested by the NNE indentation of the India plate into Asia and eastward extrusion of the Tibetan plateau, this region is tectonically active, and deforming in the form of faulting between blocks of various sizes and grand clockwise rotation around the eastern Himalaya syntax (Tapponnier and Molnar, 1977). The region is sliced by several groups of faults, among which the most prominent one is the sinistral Xianshuihe–Anninghe–Zemuhe–Xiaojiang fault system, delineating the north and east boundaries of a regional clockwise rotation around the eastern Himalaya syntax. The east–west shortening along the eastern margin of the plateau is partitioned into thrust motion along the Longmenshan fault separating Sichuan basin from the Songpan–Ganzi plateau, and dextral motion along the Longriba fault located ~150 km northwest of the Longmenshan fault (Chen et al., 2000; Shen et al., 2005). The Nanhua–Chuxiong–Jianshui, Red River, Wuliangshan, and Longling-Lancang faults are located at the southern end of the clockwise rotation, striking southeast and slipping right-laterally. Other faults in the region include the sinistral Xiaojinhe, Longling-Ruili, Dayingjiang, and Daluo-Jinghong faults striking northeast.

Accompanied with active tectonic deformation, many strong earthquakes struck the region in the past. According to the Chinese earthquake catalog composed by the Chinese Seismic Network Data Management Center (http://www.csndmc.ac.cn/newweb/index.jsp), more than 110 $M \geqslant 6.0$ events occurred in the region 1970–2013 (Fig. 1), including the 2008 Mw 7.9 Wenchuan earthquake on the Longmen Shan fault. Some of the strong earthquakes resulted in great damages and losses of human

* Corresponding author at: Department of Earth, Planetary, and Space Sciences, University of California, Los Angeles, CA 90095-1567, USA.
E-mail address: zshen@ucla.edu (Z.-K. Shen).

http://dx.doi.org/10.1016/j.jseaes.2015.04.041
1367-9120/© 2015 Elsevier Ltd. All rights reserved.

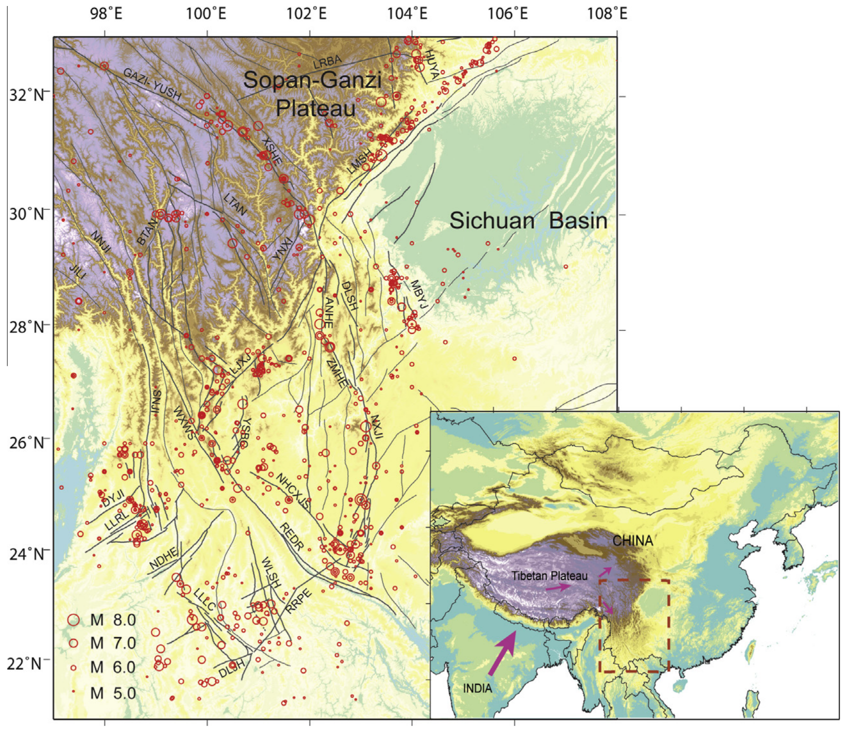

Fig. 1. Tectonic map of Sichuan-Yunnan region and $M \geqslant 5.0$ earthquakes of 1500–2013. Inset map shows geographic location of the studied region, and the arrows point to block motion directions relative to stable Eurasia plate. Earthquake data (red circles) are provided by Jie Liu of Chinese Earthquake Network Center. Abbreviations of the fault names: ANHE, Anninghe fault; BTAN, Batang fault; CLMS, Central segment of Longmenshan fault; DLJH, Daluo-Jinghong fault; DLSH, Daliangshan fault; DQZD, Deqin–Zhongdian fault; DYJI, Dayingjiang fault; ELMS, Eastern segment of Longmenshan fault; GAZI, Ganzi fault; YUSH, Yushu fault; REDR, Red River fault; HUYA, Huya fault; JILI, Jiali fault; LJXJ, Lijiang–Xiaojinhe fault; LLLC, Longling–Lancang fault; LLRL, Longling–Ruili fault; LRBA, Longriba fault; LTAN, Litang fault; MBYJ, Mabian–Yanjin fault; NHCXJS, Nanhua–Chuxiong–Jianshui fault; NNJI, Northern segment of Nujiang fault; NDHE Nandinghe fault; SNJI, Southern segment of Nujiang fault; WLSH, Wuliangshan fault; WXWS, Weixi–Weishan fault; NXJI, Northern segment of Xiaojiang fault; RRPE, Red River–Puer fault; XSHE, Xianshuihe fault; YNXI, Yunongxi fault; YSBC, Yongsheng–Binchuan fault; ZMHE, Zemuhe fault.

lives, e.g. the 1970 Mw 7.7 Tonghai earthquake caused 15621 fatalities (Han et al., 1996) and the 2008 Mw 7.9 Wenchuan earthquake resulted in more than 80,000 fatalities (http://www.gov.cn/xxgk/pub/govpublic/mrlm/200805/t20080530_32846.html), respectively. Assessment of seismic hazard potential in the region, therefore, is vitally important.

Several previous studies attempted estimation of intermediate to long term seismic potentials in the Sichuan-Yunnan region (Wen, 2001; Yi et al., 2002, 2004, 2006, 2008; Jiang and Wu, 2008; Jiang and Zhang, 2010). Using a simple point process statistics to characterize earthquake recurrence behavior, Yi et al. (2002) and Xu et al. (2005) showed that strong earthquakes in the region were clustered in time, and their recurrence times displayed no obvious periodicity. These strong events also demonstrated no characteristics of "magnitude predictable" or "time predictable" on fault segments in the region. It is, therefore, difficult to assess intermediate and long term seismic potentials based merely on observed time intervals or magnitudes of strong earthquakes on faults.

Since early 1990s, numerous statistical theorems and methods have been used for earthquake forecast and testing, and earthquake statistics has become a dynamic inter-disciplinary field for earthquake research. Kagan and Jackson (1994) first proposed an long-term earthquake forecast method based on earthquake catalog data modeling, and applied the method to seismicities in Japan (Jackson and Kagan, 1999; Kagan and Jackson, 2000), China (Rong and Jackson, 2002), and the world (Kagan and Jackson, 2011). Statistical significance of the method has been verified in these studies. Rundle et al. (2000), on the other hand, using earthquake catalog data as model constraints, developed a pattern recognition algorithm to forecast earthquakes, and applied the algorithm in California earthquake forecast. Jiang and Wu (2008) applied Rundle et al.'s (2000) method to the Sichuan-Yunnan region, and found in a retrospective test that the method had certain predictive power for mid to long term earthquake behavior in the region. Shen et al. (2007) developed a model for intermediate to long term earthquake forecast using geodetically derived strain rates map, and confirmed in a retrospective test that spatial distribution of strong earthquakes in southern California 1950–2000 correlated highly with spatial strain rate concentration. Other earthquake forecast methods, based on certain mechanical assumptions, have also been developed, for example, Keilis-Borok and Rotwain (1990) developed the TIPS (Time of Increased Probability) algorithm for mid-term large earthquake forecast, Bowman et al. (1998) proposed a method for intermediate term earthquake forecast based on regional seismicity acceleration, and Toda et al. (1998) estimated intermediate earthquake potential change after large events through calculation of Coulomb stress change and background seismicity rate. Some of these methods (e.g. Rundle et al. (2000), Keilis-Borok and Rotwain (1990), Bowman et al. (1998), and Toda et al. (1998)) are based on quite different philosophic and mechanism considerations, use fundamentally different methodologies from ours, and work on regions not covering the Sichuan-Yunnan region; we shall not discuss them further in this study.

Seismic activity is a process of energy accumulation and release, and assessment of balance between interseismic moment accumulation and coseismic moment release can be used to estimate the potential of large earthquakes (e.g. Working Group on California Earthquake Probabilities, 1995; Stein and Hanks, 1998; Ward, 1998; Meade and Hager, 2005; Wang et al., 2010; Wang et al., 2011). Wang et al. (2010) calculated the rates of seismic moment accumulation on the Longmenshan and other major faults in the northeast Tibet region using geodetic data, and compared the results with seismic moment release rate estimated from earthquake catalogs of the last 100 years. They figured that large earthquakes similar to the 2008 Mw 7.9 Wenchuan earthquake would unlikely happen in the next 50 years. Wang et al. (2011) also estimated the rates of moment accumulation on 25 major fault zones of Chinese mainland using geodetic data, and compared the result with the seismic moment released on each fault zone using the Chinese historical earthquake catalog. Their results showed that nine out of the 25 seismic zones are with large moment deficit. Their model included six fault zones but neglected some other faults in the Sichuan-Yunnan region. This study is to conduct a more detailed research on the intermediate to long term seismic potentials in this region.

We use historical earthquake catalog and geodetic deformation data to analyze seismic moment release and accumulation in the Sichuan-Yunnan region, and test three methods for seismic potential. The first one employs the earthquake catalog data only; the second one uses geodetically derived horizontal strain rates only; and the third one exploits geodetic data to estimate moment accumulation rates and earthquake catalog data to determine seismic moments released on faults, and balance the two to estimate their moment deficits and seismic potentials.

2. Methods

2.1. Seismic potential model based on spatial correlation of earthquakes

Kagan and Jackson (1994) developed an earthquake forecast model based on the assumption that probability of future earthquakes is proportional to spatial earthquake occurrence rate in the past. Following this concept, one could derive statistical models using historical earthquake catalog. Assuming that earthquake likelihood is proportional to historical earthquake rate, earthquake number-magnitude follows the Gutenberg-Richter relationship, and earthquake occurrence is a Poisson process, one could obtain the likelihood rate-density function of strong earthquakes.

According to this earthquake forecast model, the likelihood rate-density function can be factored into two functions depending independently on location and magnitude:

$$\Lambda(\theta, \varphi, m) = F(\theta, \varphi) * G(m) \quad (1)$$

where Λ is the rate of earthquake per unit area, magnitude, and time, θ and φ are latitude and longitude, m is magnitude, $F{\cdot}G = 10^{-m}$ is the normalized magnitude density distribution, and F is the spatial density function in the following form (Kagan and Jackson, 2000; Kagan and Jackson, 2011):

$$F(\theta, \varphi) = (1 - C)\sum_i \frac{1}{\pi} \frac{1}{(r_i^2 + r_s^2)} + C \quad (2)$$

where r_i is the distance between the target point (θ, φ) and the ith event, r_s is the spatial smoothing distance which involves regional tectonics, crustal thickness, and location accuracy of earthquakes, and is position dependent. C represents the uniform background seismicity.

We use an earthquake catalog to derive the seismic potential model http://www.csndmc.ac.cn/newweb/index.jsp). Information of historical earthquakes in the catalog was garnered from historical Chinese literature and field investigation. The catalog includes $M \geqslant 5.0$ earthquakes in the Sichuan-Yunnan region 1500–2013, whose time series is shown in Fig. 2a. Figs. 2b and 2c demonstrate the cumulative number of events and cumulative seismic moment

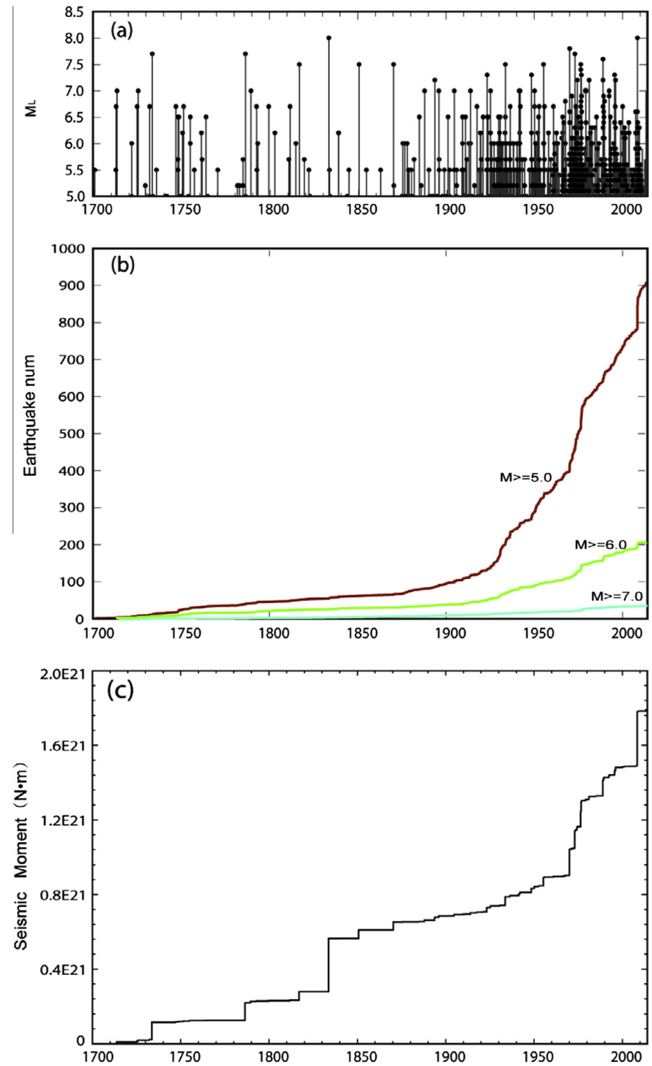

Fig. 2. (a) Earthquake magnitude time series since 1700. (b) Cumulative earthquake count for $M \geqslant 5$, $M \geqslant 6$, and $M \geqslant 7$ events, respectively. (c) Cumulative seismic moment released by earthquakes.

respectively. From Fig. 2a it is evident that many more $M < 7$ earthquakes were recorded in the last, particularly the second half of the last century than in the previous two centuries, implying that the earthquake catalog is not complete in the first 200–250 years. As shown in Fig. 2b, incompleteness of the catalog is not significant for $M \geqslant 7$ events, but is significant for $M \leqslant 7$, and particularly significant for $M \leqslant 6$ events prior to the 1930s, for which not only the mid-sized main events but also many aftershocks were not recorded without instrumental recordings. Impact of data incompleteness to seismic hazard potential estimation will be assessed in the following session.

We derive likelihood rate-density function of $M \geqslant 5.0$ earthquakes in the Sichuan-Yunnan region, using the earthquake catalog of 1500–2013 (Fig. 3). In this method each individual event is assumed to be independent of others, i.e. potential foreshocks and aftershocks are treated as independent of the main shocks. Since all the data are assigned equal weight, locations with larger events occurred would still get higher likelihood because these main shocks would have more aftershocks in its vicinity. Our result shows that the regions with highest earthquake potentials include the central segment of the Longmenshan fault and its vicinity where the 2008 Mw 7.9 Wenchuan earthquake ruptured, the

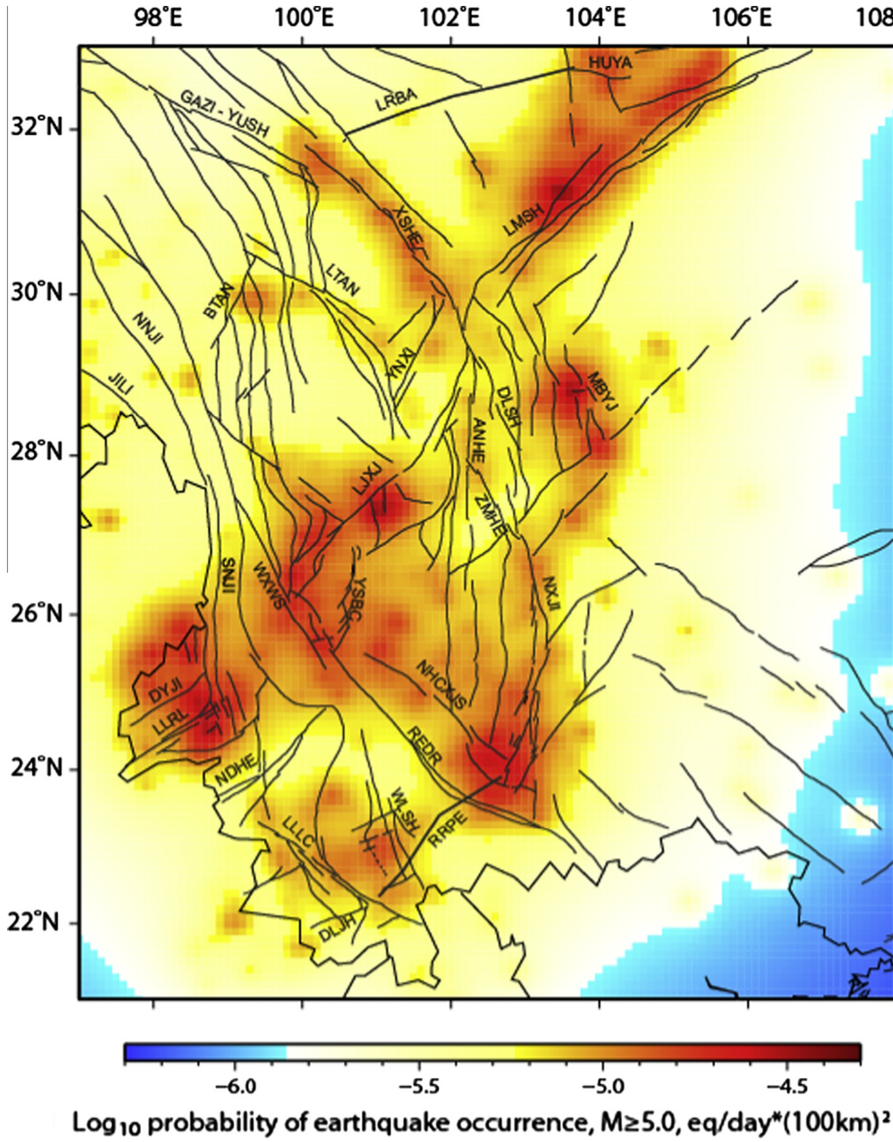

Fig. 3. Long-term earthquake potential based on earthquake catalog of 1500–2013. Acronyms of faults are the same as that in Fig. 1.

Huya, Xianshuihe, Mabian–Yanjin, and central and southern segments of the Lijiang–Xiaojinhe faults and their vicinity, and the Longling area. Other regions with high seismic potentials include the Xiaojiang, south end of the Chuxiong–Jianshui, and central segment of the Wuliangshan faults, etc. (Fig. 3).

How effective is this method in forecasting long term earthquake potentials in the Sichuan-Yunnan region? To verify validity of the method we perform two retrospective tests of the forecast result. In Test A we divide the catalog data into two sub-datasets spanning periods of 1500–1999 and 2000–2013, respectively. In Test B the data are divided into two periods different from that of Test A, 1500–1972 and 1973–2013, respectively. In both tests the first part of the dataset is used for earthquake likelihood probability density estimation, and the second part for significance test. We use error diagram to measure the efficiency of earthquake forecast algorithm. The error diagram was first suggested by Molchan (1990), similar methods were used in previous studies (e.g. Helmstetter et al., 2007; Shen et al., 2007; Kagan, 2009; Kagan and Jackson, 2011). To produce the diagram, we first divide the region into small cells ($0.5^\circ \times 0.5^\circ$ for the studied region) and estimate the theoretical forecast rate of earthquakes above a magnitude threshold for each cell. We then count the events above that magnitude threshold that actually occurred in each cell, sort the cells in the descending order of the theoretical rate, and compute the cumulative values of forecast and the observed earthquake rates. The Fig. 4b and d show the error diagrams for the two test models (Fig. 4a and c). The red curve is for the forecast, derived using seismicity data in the training period, the cells are ranked in such a way that the one with highest forecast probability is placed at the far left and the one with lowest probability at the far right, respectively. The blue curve is for cumulative number of earthquakes which occurred in the forecast period. If the assumptions on the earthquake occurrence are valid, the blue curve should be matching or above the red curve; otherwise the forecast model is not performing well.

For Test A, Fig. 4b shows that the earthquake occurrence curve is systematically below the probability density curve, meaning that the forecast of the probability model (Fig. 4a) does not fit the earthquake occurrence in the period of 2000–2013. Inspecting spatial distribution of strong earthquakes of the 14 years, we find that despite many events occurred at regions with relatively higher forecast probabilities, quite many events did occur at the low

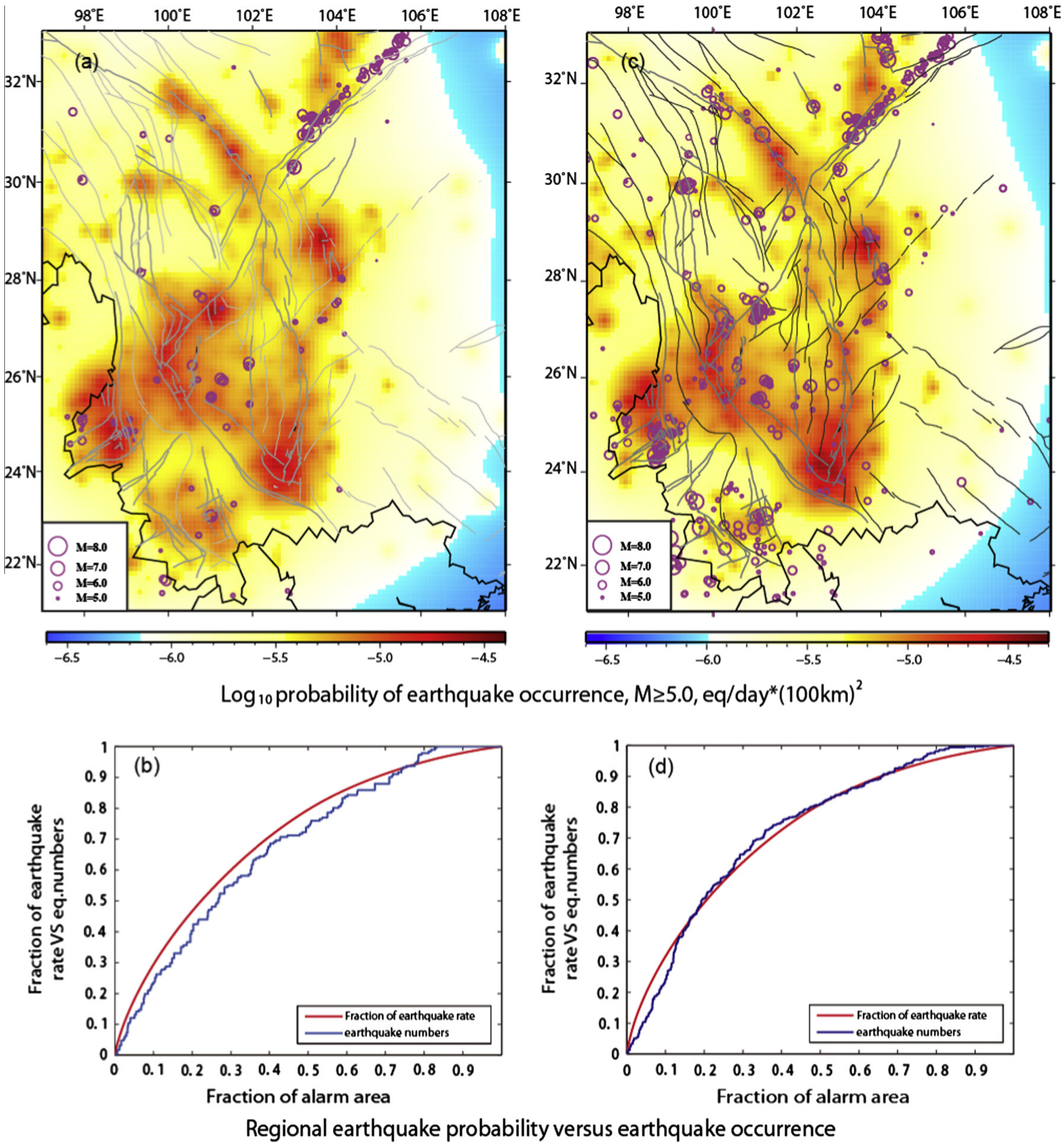

Fig. 4. Earthquake forecast Test A and Test B using earthquake catalog data. (a) Background color denotes probability density of $M \geqslant 5.0$ earthquakes forecasted using earthquake catalog of 1500–1999, and purple circles are $M \geqslant 5.0$ events occurred during 2000–2013. (b) The red and blue curves are the forecasted cumulative earthquake probability using earthquake catalog of 1500–1999 and the cumulative number of earthquakes in the 2000–2013 catalog, respectively. The cells are ranked following the forecasted earthquake probability, with the one with highest probability at the left end and the one with lowest probability at the right end, respectively. Both curves are normalized to unity. (c) and (d) are the same as that in (a) and (b) except that the forecast is made using catalog data of 1500–1972, and the test is on the earthquake catalog data of 1973–2013.

probability forecast regions, particularly the 2008 Wenchuan earthquake sequence. We suspect that the poor performance of the forecast model is resulted from incompleteness of the earthquake catalog used for the study. This circumstance is compounded with that the Longmen Shan fault has a very long recurrence time (thousands of years) (Burchfiel et al., 2008; Densmore et al., 2007; Shen et al., 2009; Zhang et al., 2010), and few strong events were ever recorded to have occurred on the fault, resulting in quite low probability predicted by the forecast model along the fault, a failure to "forecast" the Wenchuan earthquake sequence.

For Test B, it can be seen in Fig. 4d that the forecast curve is quite close to the earthquake occurrence curve. The only notable difference between the two curves is at the highest 10% probability region (at the far left side of Fig. 4d), but the gap disappears at the second highest 10% probability. The result shows that ~50% strong earthquakes occurred within the 20% highest probability region, and ~80% strong events occurred within the 50% highest probability region (for the left 50% probability in Fig. 4d). Comparison of the two test results seems to suggest that the method performs significantly better for longer period (several decades) forecast than shorter period (a decade or so) forecasting, i.e. it requires sufficient time to smooth out decadal scale fluctuations of seismicity and to yield a stable long term forecast.

In addition we calculate information scores of the two test cases based on the likelihood ratio algorithm formulated by Kagan and Knopoff (1977). Kagan and Knopoff suggested measuring the performance of the earthquake prediction algorithm by first evaluating the likelihood ratio to test how well a model approximates the actual earthquake occurrences. The information scores, I_0 and I_1, are log-likelihood ratios for forecast model and the target earthquake catalog for testing respectively, and are defined as (Kagan and Jackson, 2011):

$$I_0 = \sum_{j=1}^{N} \upsilon_j \log_2\left(\frac{\upsilon_j}{\tau_j}\right) \tag{3}$$

$$I_1 = \frac{1}{n}\sum_{i=1}^{n} \log_2\left(\frac{\lambda_i}{\xi}\right). \tag{4}$$

where j is the cell number, N is the total number of cells in the model, υ_j and τ_j are the normalized rates of occurrence and cell area, $\log_2$ is used to obtain the score in the Shannon bits of information. n is the number of earthquakes in the target catalog with i as the serial number of earthquakes, λ_i is the forecasted rate of earthquake occurrence for the cell in which the ith earthquake occurred, and ξ is a similar rate for the event occurrence according to the Poisson process with a uniform rate over region (Kagan, 2009).

The I_0 function represents the average spatial concentration of earthquake probability derived from the training earthquake catalog, and the I_1 function determines the average spatial concentration of the earthquakes in the target earthquake catalog, respectively. We compare them to investigate to what extent the actual earthquakes in the target catalog are more ($I_1 > I_0$) or less ($I_1 < I_0$) clustered in space than that in the training catalog. The results reveal that for Test A, I_1 (=0.788) is much greater than I_0 (=0.425), suggesting that the earthquake forecast does not statistically reflect the spatial occurrence rate well. However, for Test B, I_1 (=0.491) is very close to I_0 (=0.451), suggesting that the earthquake forecast does reflect the spatial occurrence rate well. We therefore conclude, similar to the conclusion of previous error diagram tests, that earthquake forecast based on such a statistic method can statistically reflect earthquake occurrence rate well when there are enough cases in the sample space; but the forecast method works well only for long term (of decades and longer) earthquake forecasts, and may not work well for short to intermediate term (of a decade and shorter) earthquake forecasts.

The two tests presented above show how incompleteness of the earthquake catalog would impact the forecast and the test results of different time periods. Fig. 2b, on the other hand, tells us that raising the cutoff magnitude will reduce the incompleteness of the catalog which is associated mainly with the smaller earthquakes. We therefore attempt another forecast model (Test C) using an earthquake catalog of $M \geqslant 6.0$ (we make no attempt with catalog of $M \geqslant 7.0$ due to the scarcity of data points retained in the catalog). The forecast model is shown in Fig. 5a. Similar to the previous forecast we perform two retrospective tests, one (case C1) with division of 1500–1999 and 2000–2013 and the other (case C2) with division of 1500–1973 and 1974–2013 as the training and test periods, respectively. The error diagram for case C1 shows much less number of events occurred in the high forecast rate region, and the cumulative event counting curve is underneath the forecast curve for the top 23% of the highest forecast rate region. For the test case C2, with an expanded test database, the test result is improved slightly, with the cumulative event counting curve underneath the forecast curve for the top 18% of the highest forecast rate region. The information scores are $I_0 = 0.553$ and $I_1 = -1.133$ for case C1 and $I_0 = 0.609$ and $I_1 = -1.234$ for case C2 respectively. Both sets of scores suggest quite different spatial concentrations of the test dataset from the training dataset. We therefore conclude that although the incompleteness of the catalog data is reduced by raising the cutoff magnitude, the number of events in the catalog is also reduced substantially, and the net result shows no significant improvement on success rate of the forecasting.

2.2. Seismic potential model based on crustal deformation field

Shen et al. (2007) developed a method using geodetic strain rate to forecast long term earthquake likelihood. In 2006 the Regional Earthquake Likelihood Models (RELM) working group of the Southern California Earthquake Center (SCEC) designed a 5-year experiment to forecast the number, spatial distribution, and magnitude distribution of subsequent $M \geqslant 5$ target earthquakes in California. A total of 17 forecasts were submitted to the RELM project (Field, 2007), among which was Shen et al.'s (2007) forecast constrained using geodetic strain rate data. A posteriori test shows that this forecast performed better than most of the other forecasts (Zechar et al., 2013).

We follow Shen et al. (2007) to assess seismic potential in the Sichuan-Yunnan region using geodetic data. This method is based on the assumptions that (a) seismicity rate is steady and proportional to the average interseismic horizontal shear strain rate, and (b) the pattern of the earthquake magnitude distribution is spatially invariant and follows a tapered Gutenberg-Richter relationship. The earthquake probability at a given spot x and magnitude M is therefore described as (Shen et al., 2007):

$$P(x, M) = A(x) \times B(M) \tag{5}$$

where $A(x)$ is proportional to the shear strain rate field and $B(M)$ is the tapered Guttenberg–Richter magnitude distribution.

The geodetic strain rate in the Sichuan-Yunnan region is derived by interpolating a GPS derived crustal motion velocity field. To determine the velocity field we processed all the available GPS data collected from 1999 to 2010 in the Sichuan-Yunnan region, and modeled GPS station position time series at each site as a function of initial position, secular velocity, and coseismic and postseismic displacements of strong earthquakes, with the postseismic displacement characterized as a logarithmic function. In our study, the 2001 Mw 7.8 Kokoxili, 2004 Mw 9.2 Sumatra, 2007 Mw 6.1 Puer, and 2008 Mw 7.9 Wenchuan earthquakes are taken into account, and the derived velocity field (showed in Fig. 4a) is expected to correspond to the secular velocity field.

Interpolation of the station velocities is done through a series of regressions, each time estimating strain and rotation rates at one site using velocity data in the neighborhood (Shen et al., 1996; Jackson et al., 1997). A locally uniform strain rate field is assumed in the process, and the velocity data are reweighted by the station azimuthal span of two azimuthally adjacent neighboring sites and the distance between a geodetic station and the site being evaluated. A Gaussian decay function $\exp(-\Delta^2/\sigma^2)$ is employed in the distance weighting function, where Δ is the site-to-station distance, and σ a smoothing distance; a greater σ means stronger smoothing in the interpolation, and vice versa. σ is determined optimally through balancing a trade-off between the formal uncertainty estimate of the strain rate and the total weight assigned to the data (see Shen et al., 2015 for details of the methodology).

Fig. 6a shows the second invariant of strain rates interpolated from the velocity field, defined as $\tau_{2inv} = \sqrt{\tau_{xx}^2 + 2\tau_{xy}^2 + \tau_{yy}^2}$, where τ_{xx}, τ_{yy}, and τ_{xy} are two normal strain rates and a shear strain rate in the east-north Cartesian coordinate, respectively. In the figure we notice that high strain rate regions are along the Xianshuihe–Xiaojiang fault and its southwest extension across the Red River fault, which we name as the Red River–Puer fault. They also span the Lijiang–Xiaojinhe fault and its southwest extension to the Longling fault, the Litang fault, the Nanhua–Chuxiong–Jianshui fault, and from the South Nujiang fault to the northwest segment of the Longling-Lancang fault. The highest strain rate is up to 100 nanostrain/year. Fig. 6a also plots $M \geqslant 6.0$ earthquakes occurred 1500 to 1972 and $M \geqslant 5.0$ events 1973–2013. It is evident from Fig. 6a that although many strong earthquakes occurred in the high

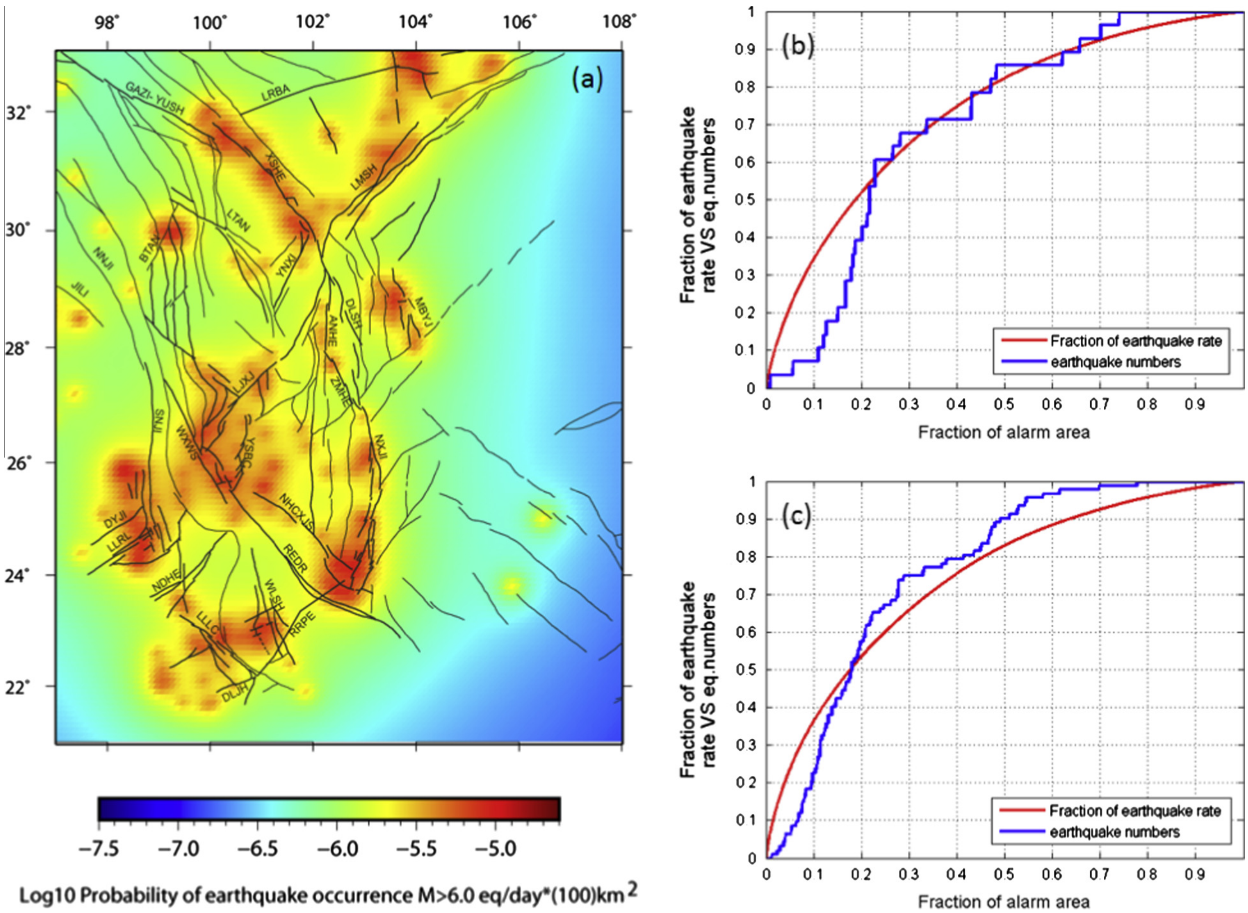

Fig. 5. Earthquake forecast Test C using $M \geqslant 6$ earthquake data. (a), (b), and (c) are similar to (a), (b), and (d) of Fig. 4, except that different earthquake catalog data are used for the forecast model constraints and tests.

strain rate regions, there are still a number of strong events, particularly the 1976 Mw 7.3 Songpan doublet sequence and the 2008 Mw 7.9 Wenchuan sequence occurred in the regions with relatively low strain rates.

To obtain a more objective understanding of the correlation between earthquake spatial distribution and strain rates, we analyze further statistics of number of earthquakes in two different time periods and the strain rates (the procedure is similar to the one used to determine error diagram in Section 2.1). The results are shown in Fig. 6b and c. To assess reliability of the result, we need to take into account uncertainties of earthquake location and magnitude measurements. Prior to the era of instrumental recording, such uncertainties may be large. The strain rate field is derived using a smoothing function with a characteristic smoothing distance of tens of kilometers, thus uncertainties in epicenter locations, usually ranging from a few to tens of kilometers, should not affect much of the result. The earthquake catalog used in this study may not be complete prior to 1900, particular for the $M < 7.0$ events. Nevertheless the method that we invoke assumes Poisson process for earthquake occurrence, therefore is sensitive to the spatial seismicity pattern that the earthquake catalog data provides but not the completeness of the catalog.

It can be seen from Fig. 6b that comparing to the strain rate forecast, distribution of the $M \geqslant 5.0$ earthquakes shows relatively more events occurred in the low strain rate regions (those cumulated at the right side of the figure) and less events occurred in the high strain rate regions (those cumulated at the left side of the figure), indicating that the geodetically derived strain rate field cannot be used as forecaster of earthquake locations of the past 41 years. The result shown in Fig. 6c, however, indicates that the spatial distribution of earthquakes since 1500 correlates well with the strain rate field, i.e. at the time interval of hundreds of years, the level of strain rates can be a good forecaster of locations of strong earthquakes. We interpret the result as that geodetically derived crustal strain rate at about decade scale reflects long term tectonic deformation field, which is mainly in the form of elastic deformation, and has to be released during earthquakes, particularly strong earthquakes. Geodetic strain rate obtained at the decade scale, therefore, may still be a good indicator of long term spatial activity of earthquakes in the region, possibly at a time scale of hundreds of years.

2.3. Seismic potential model based on joint analysis of earthquake and geodetic data for seismic moment accumulation on fault

Based on the elastic rebound theory (Reid, 1912), fault slip beneath locking depth during interseismic time period would result in elastic deformation around fault locked in upper crust, and the accumulated elastic energy would eventually be released during earthquakes. In a long run over an earthquake cycle, the elastic energy accumulated on fault would equal to the energy released during earthquakes. From fault slip rate (under locking depth) one could derive seismic moment accumulation rate, and from earthquake catalog data one could obtain history of seismic moment release. Assuming that the seismic moment accumulation rate estimated from present-day fault slip rate represents long term moment accumulation rate, by balancing total seismic moment accumulation and release on a fault, we may assess

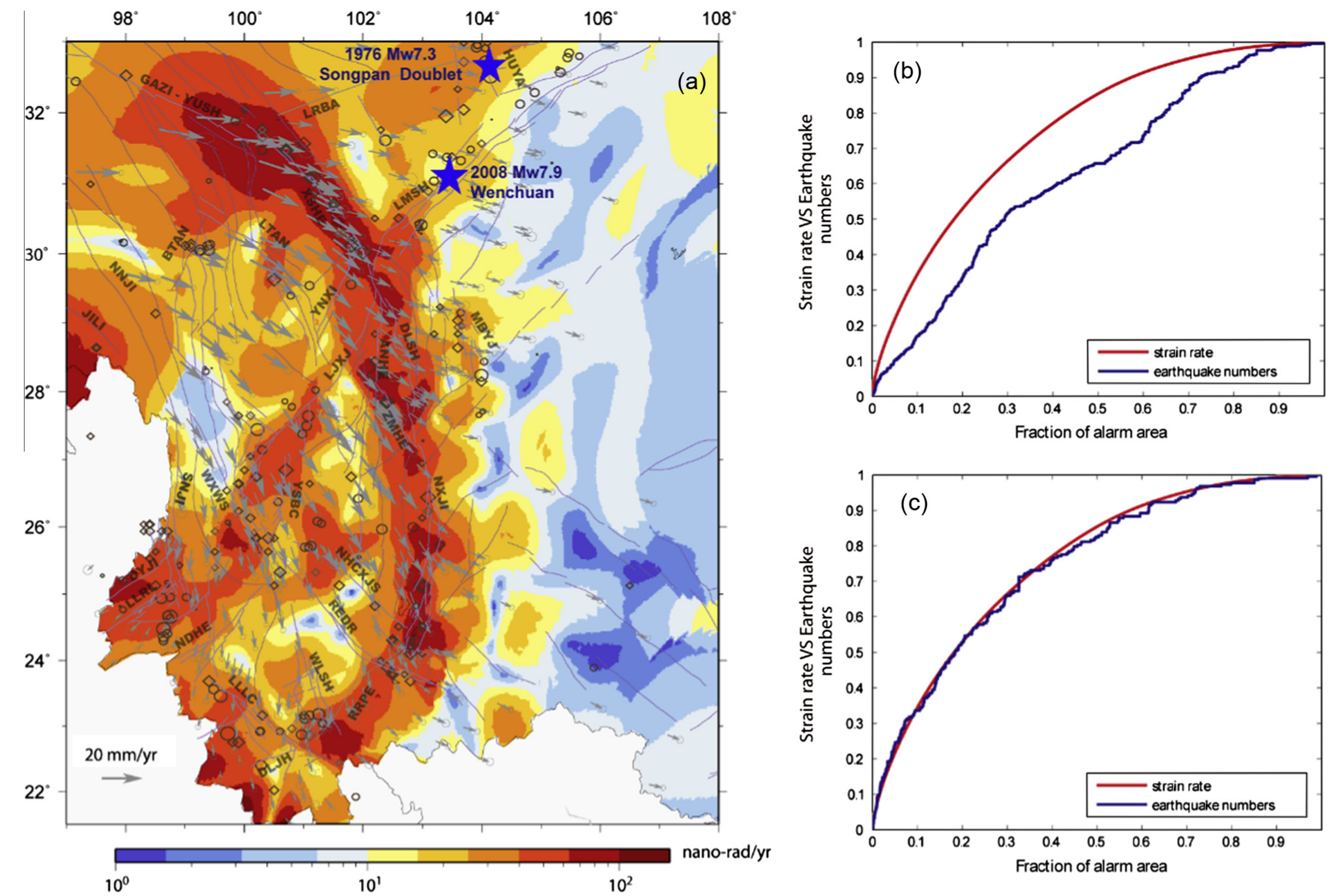

Fig. 6. (a) GPS velocity field, geodetic strain rate field and spatial distribution of strong earthquakes. The grey arrows are GPS velocity vectors with respect to the stable Eurasian reference frame, and the error ellipses represent 70% confidence. The background color shows the second invariant of strain rate. Purple diamonds and purple circles are epicenters of $M \geqslant 6.0$ events occurred during 1500–1972 and $M \geqslant 5.0$ events occurred during 1973–2013, respectively. (b). Geodetic strain rate versus earthquake count. Red curve is cumulative amount of the second invariants of strain rates in a decreasing order, and blue curve is accumulated earthquake counts of $M \geqslant 5.0$ during 1973–2013, within the corresponding regions. (c) The result for the case of $M \geqslant 6.0$ earthquakes during 1500–2013. Legends are the same as that of (b).

seismic potential on the fault based on its present-day amount of seismic moment accumulation (Working Group on California Earthquake Probabilities, 1995; Stein and Hanks, 1998; Ward, 1998; Meade and Hager, 2005).

Recurrence times of large earthquakes on faults are usually hundreds to thousands of years; and strictly speaking, budget estimation of seismic moment should account for its accumulation and release over hundreds to thousands of years. The historical earthquake records in the Sichuan-Yunnan region, however, are limited to only a few hundreds of years, and more events are missing further back in time. It is evident from Fig. 2a that although many $M < 7.5$ events are noticeably missing prior to 1900, the big ones of $M > 7.5$ are unlikely missing. This can be verified by Fig. 2b, that except a burst of M6–7 events in the 1970–1980s, the seismic moment release rate has not shown large variations for the 300-year time period. We therefore use this historic earthquake dataset and set the initial epoch of our study as 1700. For fault segments whose recurrence times are greater than 300 years our estimation results may have significant error. However, if the fault slip rates are high (>3 mm/year), our results should be relatively more accurate because these fault segments usually have shorter (about hundreds of years) recurrence intervals. We first assume that at the starting epoch of 1700 all the faults had zero moment accumulated. This assumption sometimes would lead to erroneous results, i.e. for a strong event in the historical earthquake catalog, its calculated moment release on the seismogenic fault could be greater than the moment accumulated since 1700. If such a case happens, we will adjust the starting epoch for that fault to a pre-1700 date, so that the accumulated moment during that time interval equals to the moment released by that quake. This treatment ensures no negative moment accumulations on any fault segments.

Using GPS velocity field as constraints, we develop a linked fault segment model (Wang et al., 2008; Zeng and Shen, 2014) to deduce slip rates of all the fault segments. The linked fault segment model simulates crustal deformation as caused by slips of a network of faults beneath locking depths, under the constraints of slip continuity at junctions of faults. The degree of continuity constraints is optimally determined through balancing a tradeoff between the block-like motion and individual fault slip, providing a better approximation of the real crustal deformation than the two end member models. The modeling work follows that of Wang et al. (2008) and the methodology was described in detail in Zeng and Shen (2014).

Assuming a uniform fault locking depth of 20 km and a rigidity of 3×10^{10} Pa s, we further estimate seismic moment accumulation rates and the total moments accumulated on faults (Fig. 7a). Subtracting out earthquake released moments on faults (Fig. 7b), we obtain estimates of moments accumulated on faults due to tectonic loading and earthquakes (Fig. 7c). The results are also listed in Table 1.

It can be seen from Table 1 that, although the Xianshuihe fault has the highest slip rate in the region, ~12 mm/year, a cluster of M6–7 events occurred on the fault last century has released most of the

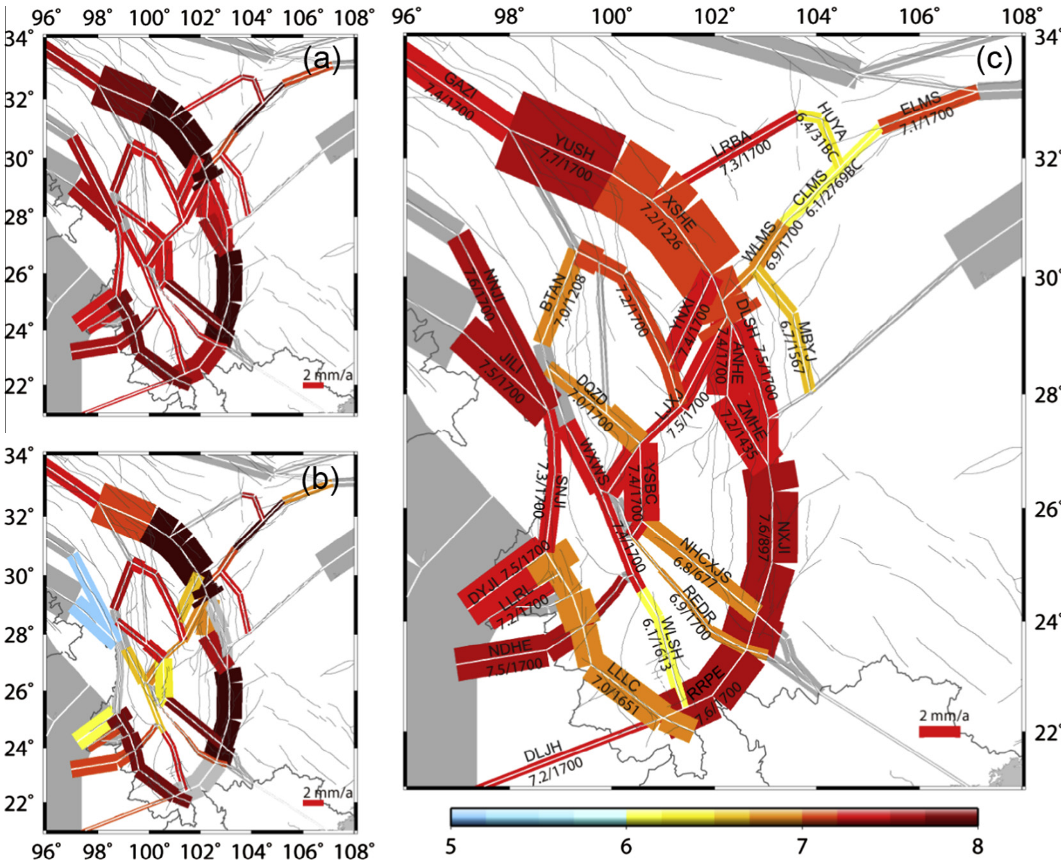

Fig. 7. Balance of seismic moment on faults. Widths of the fault segments are proportional to fault slip rates estimated by Wang et al. (2011), and colors of the fault segments denote corresponding seismic moment scaled by equivalent earthquake magnitude. (a) Predicted moment accumulation on faults up to present (the starting time may differ for individual faults, see Table 1 for detail). (b) Estimated seismic moment released on faults by earthquakes during the same periods as that of moment accumulation estimation. (c) Predicted moment deficit on faults. Numbers labeled on faults are equivalent earthquake magnitudes of moment deficits and initial time of moment accumulation.

accumulated moment, and its seismic potential right now is therefore not very high. The intersection between the Xianshuihe and Ganzi-Yushu faults shows no record of historical events, and has accumulated seismic moment of 3.6×10^{20} N m, equivalent to as large as a M7.7 earthquake. The seismic moment accumulated on the Xiaojiang fault is up to 2.9×10^{20} N m, equivalent to that released by a M7.6 event. The Daliangshan fault slips at a rate of $\sim$4 mm/year and has no historical earthquakes recorded, its accumulated seismic moment equals to a M7.5 earthquake. The Anninghe and Zemuhe faults have accumulated seismic moments equivalent to M7.4 and M7.2 earthquakes, respectively. Other high moment accumulation faults include the Jiali and Nujiang faults. The central segment of the Longmenshan fault experienced the 2008 Mw 7.9 Wenchuan earthquake which released most of the accumulated seismic moment there, and seismic potential along this fault segment therefore is not very high. The west segment of the fault was hit by the 2013 Mw 6.9 Lushan earthquake. The unreleased seismic moment on the fault segment since 1700 is enough to produce another M6.9 quake, but larger event could also occur since we have no record when the last characteristic event ruptured the fault. The east segment of the Longmenshan fault has accumulated seismic moment equivalent to at least a M7.1 earthquake.

How effective is our method in forecasting strong earthquakes? To address this question we perform a retrospective test based on historical earthquake catalog data. Considering that the early historical earthquake records suffer from greater uncertainties in location and time, our test is on the post 1900 events only. Removing aftershocks (using the method of Gardner and Knopoff, 1974), we have 69 $M \geqslant 6.0$ events left for this time period 1900–2013. For each of the 69 events, we calculate the seismic moments accumulated on all of the 32 faults at the time of the earthquake, and sort the faults in the order of moment accumulation, from highest to lowest. We then count ranking of the seismogenic fault among all the faults at the time of the event, and collect fault rankings for all the 69 events. We finally plot histogram of the number of events as function of the rankings of the faults (Fig. 8). It can be seen from Fig. 8 that, although strong events might happen at any stages of estimated seismic moment accumulation, the highest peak of the histogram is in the high ranking range, with 10 events occurred at rank 2. Also, 25 out of the 69 events ($\sim$36%) occurred in the highest ranking range ($N \leqslant 4$), which is only 13% of the total number of the faults. The result shows that these strong earthquakes occurred disproportionally in the faults with significantly higher seismic accumulation, verifying certain predictive power of the method. This method, nevertheless, has limitation that it can only be applied to faults with known characteristic event(s) occurred in the past. If the seismic moment accumulation rate on a fault is rather low and the fault experienced no large earthquakes since 1700 (such as the case of the Longmenshan fault prior to the 2008 Wenchuan earthquake), we would not know how much seismic moment had been accumulated on the fault prior to 1700, and an effective forecast could not be made.

3. Discussion and conclusions

In our first attempt of this paper we adopted approach similar to the one used by Rong and Jackson (2002), and used regional

Table 1
Seismic moment accumulation, release, and deficit on faults.

No.	Fault		Seismic moment accumulation rate			Released M_0 (N m)	Deficit moment (N m)	Equivalent Mw of deficit moment
	Fault ID	Fault name	Slip rate (mm/year)	Starting year	Accumulated M_0			
1	ANHE	Anninghe fault	8.3 ± 1.0	1700	1.6E + 20	1.3E + 20	1.5E + 20	7.4
2	BTAN	Batang fault	3.6 ± 1.2	1208	2.4E + 20	2.1E + 20	3.0E + 19	7.0
3	CLMS	Central segment of Longmenshan fault	2.1 ± 1.0	2769BC	1.1E + 21	1.1E + 21	1.3E + 21	6.1
4	DLJH	Daluo-Jinghong fault	1.3 ± 0.4	1700	1.3E + 20	5.6E + 19	7.3E + 19	7.2
5	DLSH	Daliangshan fault	4.7 ± 1.1	1700	1.9E + 20	4.1E + 17	1.9E + 20	7.5
6	DQZD	Deqin-Zhongdian fault	3.5 ± 1.0	1700	1.1E + 20	8.0E + 19	3.4E + 19	7.0
7	DYJI	Dayingjiang fault	6.9 ± 1.5	1700	1.9E + 20	2.2E + 18	1.8E + 20	7.5
8	ELMS	East segment of Longmenshan fault	2.6 ± 1.2	1700	6.9E + 19	2.4E + 19	4.5E + 19	7.1
9	GAZI	Ganzi fault	5.0 ± 0.8	1700	3.0E + 20	1.6E + 20	1.4E + 20	7.4
10	YUSH	Yushu fault	13.9 ± 0.9	1700	4.0E + 20	4.0E + 19	3.6E + 20	7.7
11	REDR	Red River fault	1.4 ± 1.3	1700	7.2E + 19	4.4E + 19	2.8E + 19	6.9
12	HUYA	Huya fault	1.9 ± 1.3	31BC	2.4E + 20	2.4E + 20	4.4E + 18	6.4
13	JILI	Jiali fault	7.5 ± 1.5	1700	2.3E + 20	4.2E + 16	2.3E + 20	7.5
14	LJXJ	Lijiang-Xiaojinhe fault	3.3 ± 1.1	1700	1.9E + 20	1.8E + 19	1.8E + 20	7.5
15	LLLC	Longling-Lancang fault	6.0 ± 1.4	1651	4.8E + 20	4.5E + 20	3.0E + 19	7.0
16	LLRL	Longling-Ruili fault	4.6 ± 2.2	1700	1.1E + 20	3.6E + 19	7.2E + 19	7.2
17	LRBA	Longriba fault	1.9 ± 0.4	1700	8.4E + 19	2.0E + 15	8.4E + 19	7.3
18	LTAN	Litang fault	3.3 ± 1.2	1700	1.7E + 20	1.0E + 20	6.8E + 19	7.2
19	MBYJ	Mabian-Yanjin fault	2.3 ± 0.8	1567	1.2E + 20	1.1E + 20	1.1E + 19	6.7
20	NHCXJS	Nanhua-Chuxiong-Jianshui fault	3.8 ± 0.4	677	6.6E + 20	6.5E + 20	1.9E + 19	6.8
21	NNJI	North segment of Nujiang fault	4.8 ± 0.9	1700	2.5E + 20	4.8E + 16	2.5E + 20	7.6
22	NDHE	Nandinghe fault	4.6 ± 1.4	1700	2.5E + 20	3.5E + 19	2.2E + 20	7.5
23	SNJI	South segment of Nujiang fault	2.8 ± 1.4	1700	1.1E + 20	1.8E + 16	1.1E + 20	7.3
24	WLSH	Wuliangshan fault	2.3 ± 1.1	1613	1.0E + 20	1.0E + 20	1.7E + 19	6.1
25	WXWS	Weixi-Weishan fault	3.0 ± 0.8	1700	1.5E + 20	6.6E + 18	1.5E + 20	7.4
26	NXJI	North segment of Xiaojiang fault	10.0 ± 1.1	897	1.9E + 21	1.6E + 21	2.9E + 20	7.6
27	RRPE	Red River–Puer fault	8.8 ± 1.7	1700	2.8E + 20	2.9E + 16	2.8E + 20	7.6
28	XSHE	Xianshuihe fault	12.5 ± 1.4	1226	1.6E + 21	1.6E + 21	6.9E + 19	7.2
29	YNXI	Yunongxi fault	4.8 ± 1.0	1700	1.3E + 20	6.2E + 18	1.2E + 20	7.4
30	YS-BC	Yongsheng-Binchuan fault	6.0 ± 1.3	1700	1.6E + 20	4.4E + 18	1.6E + 20	7.4
31	ZMHE	Zemuhe fault	7.2 ± 1.2	1435	2.9E + 20	2.1E + 20	8.2E + 19	7.2
32	WLMS	Western segment of Longmenshan fault	2.4 ± 0.9	1700	6.3E + 19	3.5E + 19	2.8E + 19	6.9

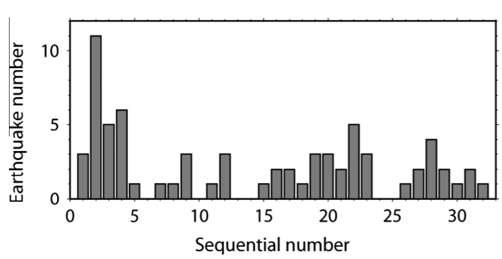

Fig. 8. Number of earthquakes occurred on fault versus ranking of seismic moment accumulation on fault. The rankings are based on moment deficits on faults at the time of an earthquake, and are placed in a descending order.

seismicity data to constrain earthquake probability model. Major differences between the two studies are that Rong and Jackson studied a region spanning the Chinese continent, and used earthquake catalog data starting in 1900 with a cut-off magnitude of M5.4; while our studied region is only the southwest part of the Chinese continent, and the earthquake catalog we used starting in 1500 with a cut-off magnitude of M5.0. Considering that the earthquake recurrence times in China are usually hundreds, and sometimes even thousands of years, using a longer time span of the earthquake catalog data, even somewhat incomplete for early years, should yield more precise estimates of long term earthquake potential. Due to difference in parameterization, the two models cannot be strictly compared with. Nevertheless, retrospective test of our model's 'forecast' (shown in Fig. 4d) seems to agree with data better than that of Rong and Jackson's (Fig. 3 of their paper), attesting that goodness of forecast relies heavily on earthquake catalog, the longer and more complete the historical earthquake catalog is, the more reliable the forecast will be. This method, therefore, is more promising to be used in China and other countries which have relatively longer records of historical earthquakes for long term earthquake forecasts.

Our second approach is to use secular geodetic strain rate deduced from GPS velocity data to derive intermediate to long term earthquake probability. Retrospective test of the probability model with earthquake occurrence of the past 30 years shows that the model 'forecasted' poorly. However, the model seems to 'forecast' spatial intensity of earthquakes for the past 500 years reasonably well, suggesting that the geodetic strain rate obtained at the decadal scale may still be a good indicator of long term earthquake activity in the region, but only at a time scale of hundreds of years.

Comparing results from our first and second attempts, we find that the 'forecasts' for the time period 1973–2013 using earthquake catalog data are significantly better than that using geodetic strain rate data. Nevertheless the geodetic 'forecasts' for the past 500 years work equally well as the 'forecasts' using earthquake catalog data for the 41 years of 1973–2013. We interpret this as perhaps due to the fact that geodetic strain rates reflect primarily a steady process of long term tectonic strain build-up, which is better correlated with earthquake occurrences of hundreds to thousands of years. The seismic moment release, however, is a process of both Poisson and clustering (Jackson and Kagan, 1999). The earthquake catalog dataset, owning to the fulfilment of instrumental recording, picks up many more M5–6 events since 1930's than before, and their clustering effect with the testing events of 1973–2013 in the catalog may play a role for its 'forecasts' outperforming the ones obtained using geodetic strain rate data in the same testing time period range.

In our third attempt, we used geodetically derived fault slip rates to estimate the seismic moment accumulation rates on major active faults, and compared the results with the seismic moments released since 1700 to evaluate the corresponding earthquake potentials.

Doing so requires a long and ideally complete record of past strong earthquakes. Although the result may not be so reliable for faults with slower slip rates and longer recurrence times, it seems doing a reasonable job for the ones with faster slip rates and shorter recurrence times, evidenced by our retrospective test shown in Fig. 8. Though we have adopted longer durations for estimating seismic moment accumulation than those in Wang et al. (2011), accumulated seismic moments we forecast at some faults are still lower than that of Wang et al. (2011). For example, our model measures seismic moment accumulated on the Red River fault which is equivalent to an M6.9 earthquake (seismic moment accumulation duration 1700–2013), but it is estimated as an M7.4 event in Wang et al.'s model (seismic moment accumulation duration 1880–2010). Also the estimate for the Longling-Lancang fault is an M7.0 event for our model (seismic moment accumulation duration: 1653–2013) and an M7.1 event for Wang et al.'s (marked as the Lancang River fault, seismic moment accumulation duration 1850–2010), respectively. The main reasons for the differences are that: (a) Wang et al.'s model covered the entire Chinese continent and delineation of fault zones is not as detailed as ours in the Sichuan-Yunnan region. Some individual faults in their model therefore represent combinations of multiple faults in our model. For example, the Anninghe–Xiaojiang fault in their model equals to the suite of the Anninghe, Zemuhe, Daliangshan, and Xiaojiang faults in our model. Because our model accounts more variations in fault geometry and slip rates based on more detailed studies, our result should have better resolution and assessments of seismic potential on individual faults. (b) The starting epochs of cumulative seismic moments on faults of the two studies are also quite different. The starting epochs in our model are 1700 or earlier, while the ones used by Wang et al. for the six faults in the Sichuan-Yunnan region are between 1600 and 1850. We chose the starting epochs based on the completeness of the regional historical earthquake catalog and positivity of seismic moment accumulation on faults, and the values should be more suitable for the regional study.

Our result of the third approach suggests that numerous faults in the Sichuan-Yunnan region have accumulated seismic moments capable of producing $M > 7.5$ earthquakes, including the Xiaojiang, Jiali, Northern Nujiang, Nandinghe, Red River–Puer faults, and the junction fault between the Xianshuihe and Ganzi-Yushu faults.

Acknowledgments

We thank Editor-in-Chief Bor-ming Jahn and Editor Dapeng Zhao for their handling of the manuscript, and Corne Kreemer and an anonymous reviewer for their thoughtful and constructive comments. This research was supported by the China Earthquake Administration (200708002) and the National Science Foundation of China (41090294). It was also supported by a NSF I/RD grant (EAR-1323052) for Z.-K. Shen as a rotator program director at NSF. Any opinion, findings, and conclusions or recommendations expressed in this material are those of the author(s) and do not necessarily reflect the views of the National Science Foundation.

References

Bowman, D.D., Ouillon, G., Sammis, C.G., Sornette, A., Sornette, D., 1998. An observational test of the critical earthquake concept. J. Geophys. Res. 103 (B10), 24359–24372.

Burchfiel, B.C., Royden, L.H., Van der Hilst, R.D., Hager, B.H., Chen, Z., King, R.W., Li, C., Lü, J., Yao, H., Kirby, E., 2008. A geological and geophysical context for the Wenchuan earthquake of 12 May 2008, Sichuan, People's Republic of China. GSA Today 18 (7).

Chen, Z., Burchfiel, B.C., Liu, Y., King, R.W., Royden, L.H., Tang, W., Wang, E., Zhao, J., Zhang, X., 2000. Global Positioning System measurements from eastern Tibet and their implications for India/Eurasia intercontinental deformation. J. Geophys. Res. 105 (B7), 16215–16227.

Densmore, A.L., Ellis, M.A., Li, Y., Zhou, R., Hancock, G.S., Richardson, N., 2007. Active tectonics of the Beichuan and Pengguan faults at the eastern margin of the Tibetan Plateau. Tectonics 26, TC4005.

Field, E.H., 2007. Overview on the working group for the development of Regional Earthquake Likelihood Models (RELM). Seismol. Res. Lett. 78, 7–16.

Gardner, J.K., Knopoff, L., 1974. Is the sequence of earthquakes in southern California, with aftershocks removed, Poissonian. Bullet. Seismolog. Soc. Am. 64, 1363–1367.

Han, X.M., Mao, Y.P., Zhou, R.Q., 1996. Study of casualties on Tonghai M7.7 earthquake in 1970. J. Seismol. Res. 19, 199–205 (in Chinese).

Helmstetter, A., Kagan, Y.Y., Jackson, D.D., 2007. High-resolution time-independent grid-based forecast for M $\geqslant$ 5 earthquakes in California. Seismol. Res. Lett. 78, 78–86.

Jackson, D.D., Kagan, Y.Y., 1999. Testable earthquake forecasts for 1999. Seismol. Res. Lett. 70, 393–403.

Jackson, D.D., Shen, Z.-K., Potter, D., Ge, X.B., Sung, L., 1997. Southern California deformation. Science 277, 1621–1622.

Jiang, C.S., Wu, Z.L., 2008. Retrospective forecasting test of a statistical physics model for earthquakes in Sichuan-Yunnan region. Sci. China, Ser. D Earth Sci. 51, 1401–1410.

Jiang, C.S., Zhang, J.C., 2010. Evaluation of background seismicity and potential source zones of strong earthquakes in the Sichuan-Yunan region based on the space-time ETAS model. Acta Geophys. 53, 305–317 (in Chinese).

Kagan, Y.Y., 2009. Testing long-term earthquake forecasts: likelihood methods and error diagrams. Geophys. J. Int. 177, 532–542.

Kagan, Y.Y., Jackson, D.D., 1994. Long-term probabilistic forecasting of earthquakes. J. Geophys. Res. 99 (B7), 13685–13700.

Kagan, Y.Y., Jackson, D.D., 2000. Probabilistic forecasting of earthquakes. Geophys. J. Int. 143, 438–453.

Kagan, Y.Y., Jackson, D.D., 2011. Global earthquake forecasts. Geophys. J. Int. 184, 759–776.

Kagan, Y.Y., Knopoff, L., 1977. Earthquake risk prediction as a stochastic process. Phys. Earth Planet. Interiors 14, 97–108.

Keilis-Borok, V.I., Rotwain, I.M., 1990. Diagnosis of time of increased probability of strong earthquakes in different regions of the world: algorithm CN. Phys. Earth Planet. Inter. 61, 57–72.

Meade, B.J., Hager, B.H., 2005. Spatial localization of moment deficits in southern California. J. Geophys. Res. 110, B4402.

Molchan, G.M., 1990. Strategies in strong earthquake prediction. Phys. Earth Planet. Inter. 61, 84–98.

Reid, H.F., 1912. The elastic-rebound theory of earthquakes. Bull. Seismol. Soc. Am. 2, 98–100.

Rong, Y., Jackson, D., 2002. Earthquake potential in and around China: estimated from past earthquakes. Geophys. Res. Lett. 29 (16), 21–27. http://dx.doi.org/10.1029/2002GL015297.

Rundle, J.B., Klein, W., Turcotte, D.L., Malamud, B.D., 2000. Precursory seismic activation and critical-point phenomena. Pure Appl. Geophys. 157, 2165–2182.

Shen, Z.-K., Jackson, D.D., Ge, X.B., 1996. Crustal deformation across and beyond the Los Angeles basin from geodetic measurements. J. Geophys. Res. 101, 27927–27980.

Shen, Z.-K., Lü, J., Wang, M., Bürgmann, R., 2005. Contemporary crustal deformation around the southeast borderland of the Tibetan Plateau. J. Geophys. Res. 110, B11409. http://dx.doi.org/10.1029/2004JB003421.

Shen, Z.-K., Jackson, D.D., Kagan, Y.Y., 2007. Implications of geodetic strain rate for future earthquakes, with a five-year forecast of M5 earthquakes in southern California. Seismol. Res. Lett. 78, 116–120.

Shen, Z.-K., Sun, J., Zhang, P., Wan, Y., Wang, M., Bürgmann, R., Zeng, Y., Gan, W., Liao, H., Wang, Q., 2009. Slip maxima at fault junctions and rupturing of barriers during the 2008 Wenchuan earthquake. Nat. Geosci. 2, 718–724.

Shen, Z.-K., Wang, M., Zeng, Y., Wang, F., 2015. Optimal interpolation of spatially discretized geodetic data. Bullet. Seismolog. Soc. Am., submitted for publication.

Stein, R.S., Hanks, T.C., 1998. M $\geqq$ 6 earthquakes in southern California during the twentieth century: no evidence for a seismicity or moment deficit. Bull. Seismol. Soc. Am. 88, 635–652.

Tapponnier, P., Molnar, P., 1977. Active faulting and tectonics in China. J. Geophys. Res. 82, 2905–2930.

Toda, S., Stein, R.S., Reasenberg, P.A., Dieterich, J.H., Yoshida, A., 1998. Stress transferred by the 1995 Mw = 6.9 Kobe, Japan, shock: effect on aftershocks and future earthquake probabilities. J. Geophys. Res. 103, 24543–24565.

Wang, Y.Z., Wang, E.N., Shen, Z.-K., Wang, M., Gan, W.J., Qiao, X.J., Meng, G.J., Li, T.M., Tao, W., Yang, Y.L., 2008. GPS-constrained inversion of present-day slip rates along major faults of the Sichuan-Yunnan region, China. Sci. China, Ser. D Earth Sci. 51, 1267–1283.

Wang, H., Liu, M., Shen, X., Liu, J., 2010. Balance of seismic moment in the Songpan-Ganze region, eastern Tibet: implications for the 2008 Great Wenchuan earthquake. Tectonophysics 491, 154–164.

Wang, H., Liu, M., Cao, J., Shen, X., Zhang, G., 2011. Slip rates and seismic moment deficits on major active faults in mainland China. J. Geophys. Res. 116, B2405.

Ward, S.N., 1998. On the consistency of earthquake moment rates, geological fault data, and space geodetic strain: the United States. Geophys. J. Int. 134, 172–186.

Wen, X.Z., 2001. Earthquake behavior of variable rupture-scale on active faults and application of the cascade-rupturing model. Acta Seismoiogica Sinica 23, 380–390 (in Chinese).

Working Group on California Earthquake Probabilities, 1995. Seismic hazards in southern California: probable earthquakes, 1994–2024. Bullet. Seismolog. Soc. Am. 85, 378–439

Xu, X.W., Zhang, P.Z., Wen, X.Z., Qin, Z.L., Chen, G.H., Zhu, A.L., 2005. Features of active tectonics and recurrence behaviors of strong earthquakes in the western Sichuan province and its adjacent regions. Seismol. Geol. 27, 446–461 (in Chinese).

Yi, G.X., Wen, X.Z., Xu, X.W., 2002. Study on recurrence behaviors of strong earthquakes for several entireties of active fault zones in Sichuan-Yunnan region. Earthquake Res. China 18, 267–276 (in Chinese).

Yi, G.X., Wen, X.Z., Fan, J., Wang, S., 2004. Assessing current faulting behaviors and seismic risk of the Anninghe-Zemuhe fault zone from seismicity parameters. Acta Seismol. Sin. 17, 322–333 (in Chinese).

Yi, G.X., Wen, X.Z., Wang, S.W., Long, F., Fan, J., 2006. Study on fault sliding behaviors and strong-earthquake risk of the Longmenshan-Minshan fault zones from current seismicity parameters. Earthquake Res. China 22, 117–125 (in Chinese).

Yi, G.X., Wen, X.Z., Sun, Y.J., 2008. Study on the potential strong-earthquake risk for the eastern boundary of the Sichuan-Yunnan active faulted-block, China. Chin. J. Geophys. 51, 1151–1158 (in Chinese).

Zechar, J.D., Schorlemmer, D., Werner, M.J., Gerstenberger, M.C., Rhoades, D.A., Jordan, T.H., 2013. Regional earthquake likelihood models I: first-order results. Bull. Seismol. Soc. Am. 103 (2A), 787–798. http://dx.doi.org/10.1785/0120120186.

Zeng, Y., Shen, Z.-K., 2014. Fault network modeling of crustal deformation in California constrained using GPS and geologic observations. Tectonophysics 612, 1–17.

Zhang, P.Z., Wen, X., Shen, Z.-K., Chen, J., 2010. Oblique, high-angle, listric-reverse faulting and associated development of strain: the Wenchuan earthquake of May 12, 2008, Sichuan, China. Annu. Rev. Earth Planet. Sci. 38, 353–382.